ACS Catalysis

RESEARCH ARTICLE

pubs.acs.org/acscatalysis

Modifying the Size of Nickel Metallic Particles by H_2/CO Treatment in Ni/ZrO_2 Methane Dry Reforming Catalysts

Victor M. Gonzalez-Delacruz, Rosa Pereñiguez, Fatima Ternero, Juan P. Holgado, and Alfonso Caballero*

Instituto de Ciencia de Materiales de Sevilla, CSIC-University of Seville, and Departamento de Quimica Inorganica, University of Seville, Avda. Américo Vespucio 49, 41092 Seville, Spain

ABSTRACT: The effect of a reduction process with CO or H_2 on the size of nickel particles in Ni/ZrO_2 dry methane reforming catalysts have been studied by means of in situ X-ray Absorption Spectroscopy (XAS) and Diffuse Reflectance FTIR Spectroscopy (DRIFTS). Our results clearly indicate that a high temperature treatment with CO increases the dispersion of the nickel metallic phase. XAS results have shown a lower coordination number of Ni in the sample treated with CO than that reduced with H_2. From the DRIFTS results, it can be established that, under the CO treatment, the formation of $Ni(CO)_4$ complexes corrodes the nickel particles, decreasing their size. The formation of these gas molecules occurs without measurable losses of nickel from the catalyst which maintains the same nickel content after the hydrogen or the CO treatment at high temperature. Therefore, this airborne nickel compound, by colliding with the zirconia surface, must deposit the nickel metal atoms around onto the support. This behavior is evidence of an important interaction between nickel and zirconia surface as unlike other supports there is no losses of nickel during the dispersion process on zirconia. Although different effects of CO on nickel catalysts have been previously described, we have found for the first time several experimental evidences demonstrating the whole redispersion phenomenon.

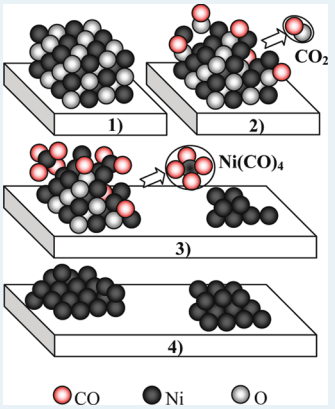

KEYWORDS: nickel catalysts, XAS, FTIR, DRIFTS, dispersion, dry methane reforming, reduction with CO

1. INTRODUCTION

Reforming of methane is at present one of the most important industrial reactions, partially because of the huge reserves of natural gas.[1,2] Nowadays, Ni-based catalysts continue as the best economic and performing catalytic systems for this kind of hydrocarbon reforming reactions,[3−5] and in particular for the steam reforming of methane, which has been proposed as the source for hydrogen production.[6] Beside this reaction, the dry reforming of methane, using carbon dioxide as oxidant, has been lately extensively studied as an alternative, even though it has been pointed out as impractical for commercial hydrogen generation.[7] In spite of that, there is a great potential in the application of CO_2 reforming of methane in environmental areas, such as the elimination of CO_2 emissions from natural gas deposits or the utilization of these two greenhouse gases for obtaining synthesis gas (CO/H_2)[8,9] which, in different proportions, is extensively used in industrial processes as methanol synthesis, hydrogenations, or Fischer−Tropsch reactions.[10]

However, these kinds of Ni-based materials are very sensitive to the coke deposition during reaction, which hinders their use as a long-term catalyst in industrial applications. Several papers have stated that the dispersion, morphology, and interaction of the nickel metallic phase with the support strongly determine the catalytic performances of these catalysts.[11−14] In general, it has been established the difficulty in preparing Ni-based catalysts of appropriate dispersion and stability.

As fresh nickel catalysts usually present the oxide phase, a previous reduction process is needed to obtain the catalytic active phase of nickel before performing the reaction. This previous step, essential for obtaining an appropriate final dispersion of the reduced metallic phase, is therefore one of the most important stages in the preparation process. As the pretreatment of the catalysts with H_2 is the most common process of reduction, Ni-based catalysts have been extensively studied during this process showing in some cases the existence of strong interactions between the Ni particles and the support.[13,15] On the other hand, a number of previous investigations have shown that under certain conditions, CO corrosively interacts with metallic nickel, causing changes on the metal particles sizes and even some nickel loss from the catalyst surface.[16] This effect is especially relevant in hydrocarbon reforming reactions, as beside hydrogen, CO is formed as a product. Sintering of the Ni particles during treatments with CO has also been reported by some authors.[16−19] All these effects have been assumed to be caused by nickel transport from particle to particle in the form of nickel sub/tetracarbonyls which migrate either on the support surface or through the gas phase, leading to the metal particles growth. In this work, we have studied the effect of two different processes of reduction, with H_2 or with CO, in the metallic particle sizes of two different Ni/ZrO_2 catalysts active for the dry reforming reaction of methane (DRM). The use of different characterization techniques, such as X-ray diffraction (XRD), Scanning Electron Microscopy (SEM), and in situ X-ray Absorption

Received: December 3, 2010
Revised: December 16, 2010
Published: January 18, 2011

Spectroscopy (XAS) and Diffuse Reflectance FTIR Spectroscopy (DRIFTS), has allowed us to determine and compare the relative size of the nickel particles achieved by the two different reduction processes.

2. EXPERIMENTAL SECTION

Catalysts Preparation. Two different nickel loadings were used to obtain diverse particles size and metal dispersions. A 26 wt % Ni/ZrO_2 and a 3 wt % Ni/ZrO_2 catalytic systems were prepared as powder by impregnation of a monoclinic zirconia support with a nickel nitrate solution ($Ni(NO_3)_2 \cdot 6H_2O$ from Aldrich). Zirconia support was synthesized via forced hydrolysis[20] using an aqueous solution of $ZrO(NO_3)_2 \cdot xH_2O$ (from Aldrich). The powder was calcined at 850 °C during 3 h to prevent any change on the support under reaction temperatures.

Temperature Programmed Reduction (TPR). TPR experiments were done from room temperature up to 500 °C, with a heating rate of 10 °C/min, holding temperature at 500 °C for 1 h. A thermal conductivity detector (TCD), previously calibrated using CuO, and a mass spectrometer in line with the TCD, calibrated with reference mixtures, were used to detect variations of reducing agent concentration, and possible subproducts formation. A H_2/Ar mixture (5% H_2, 50 mL/min flow) was used for H_2-reduction, while reduction with CO was accomplished with a 5% CO/He mixture. All the experimental conditions were chosen to ensure that no peak coalescence occurs.[21]

Catalytic Activity Tests. Reaction was carried out in a fixed-bed tubular reactor described elsewhere,[22] using 40 mg of catalysts between two pompons of quartz wool. Before reaction, samples were reduced with CO or H_2 at 500 °C during 1 h. The CH_4 and CO_2 reactants were mixed at a ratio of 1 diluted in He (10:10:80 in volume). Samples were heated from room temperature up to 750 at 1 °C/min rate, held at 750 °C during 12 h, and finally cooled down to room temperature in the same reaction mixture. Reactants and products were analyzed by means of a gas chromatograph (Varian, CP-3800) equipped with a thermal conductivity detector (TCD) and a Porapak Q packed column.

XRD and SEM. X-ray diffractograms were recorded in a Panalytical XPert PRO device, equipped with a X'Celerator Detector (active range of $2\theta = 2.18°$), with a Bragg−Brentano configuration, using Cu Kα ($\lambda = 1.5418$ A). Diagrams were collected in the range $2\theta = 20°-80°$, with a step of 0.05° and an acquisition time of 80 s for each point. To calculate the mean size of the crystalline particles of Nickel and nickel oxide by Scherrer formula, X-ray diffractograms were also collected in the range of $2\theta = 35°-55°$, with a step of 0.03° during 100 s each point. SEM images were obtained in a Hitachi S-5200 microscope equipped with a field emission filament, using an accelerating voltage of 5 kV.

XAS. X-ray absorption spectra were recorded at the BM25 beamline (SPLINE) of the ESRF synchrotron (Grenoble, France). The spectra were acquired in transmission mode, using self-supported wafers of the Ni/ZrO_2 sample, in a modified commercial infrared cell (Specac) able to work up to 800 °C under controlled atmosphere.[13] XAS spectra were collected at different temperatures during treatments of the samples.

In all cases the self-supported pellets were prepared using the optimum weight to maximize the signal-to-noise ratio in the ionization chambers ($\log I0/I1 \approx 1$). Mass flow controllers were used for dosing the gases to the cell. The composition of the gas mixtures were similar to that previously used in the TPR experiment during the hydrogen or CO reduction treatments. For energy calibration, a standard Ni foil was introduced after the second ionization chamber ($I1$) and measured simultaneously. Typical XAS spectra of Ni K-edge were recorded from 8200 to 9100 eV, with a variable step energy value, with a minimum 0.5 eV step across the XANES region. Once extracted from the XAS spectra, the EXAFS oscillations were Fourier transformed in the range 2−11.0 $Å^{-1}$. Spectra were analyzed using the software package IFEFFIT.[23] The theoretical paths for Ni−Ni and Ni−O species used for fitting the first coordination shell of the experimental data were generated using the ARTEMIS program and the FEFF 7.0 program.[24] The coordination number, interatomic distance, Debye−Waller factor and inner potential correction were used as variable parameters for the fitting procedures. Reference spectra for metallic Ni and NiO were recorded using standard reference samples.

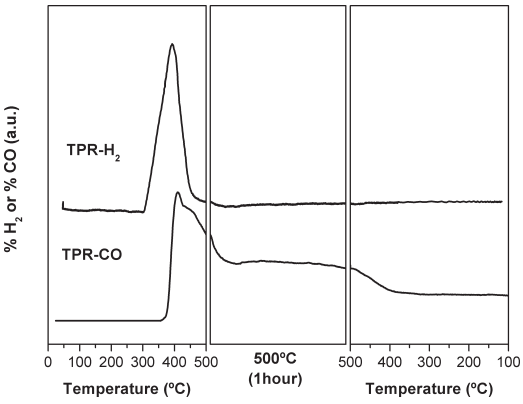

Figure 1. TPR profiles of 26 wt % Ni/ZrO_2 system, reduction with H_2 (upper profile) and reduction with CO (down). Experiments were carried out from room temperature to 500 °C at a heating rate of 10 °C/min, holding the sample at 500 °C during 1 h.

DRIFTS. FTIR spectra were collected in a FTIR JASCO 6300 equipped with a Praying Mantis DRIFTS cell, using a reaction chamber able to work up to 600 °C under controlled atmosphere. Mass flow controllers were utilized for dosing the gases to the chamber, passing through the powder sample. FTIR spectra were collected in the range of 4000−700 cm^{-1} with a resolution of 4 cm^{-1} and 100 scans each. Spectra were acquired at different temperatures during the "in situ" treatment of the sample.

3. RESULTS AND DISCUSSION

3.1. TPR. The processes of reduction of the 26 wt % Ni/ZrO_2 catalyst with H_2 or CO were studied by TPR experiments. According to the data obtained by these experiments, depicted in Figure 1, the main reduction peaks are similar in shape, in both cases centered around 400 °C. The total H_2 consumption until 500 °C roughly corresponds to that expected for the complete reduction of the NiO phase to metallic Ni^0. However, when reduced with CO, the consumption of this reducing agent is much higher than expected, mainly because of the presence of a wide new peak around 500 °C. As a subsequent oxidation treatment produces a large amount of CO_2, this peak must be due to the decomposition of CO through the Boudouard reaction ($2CO \rightarrow C + CO_2$). In fact, as it will be shown in section 3.4, the SEM images obtained after this CO treatment confirm the presence of carbon in the CO-reduced catalyst, which is completely eliminated by oxidation at 500 °C.

dx.doi.org/10.1021/cs100116m |ACS Catal. 2011, 1, 82–88

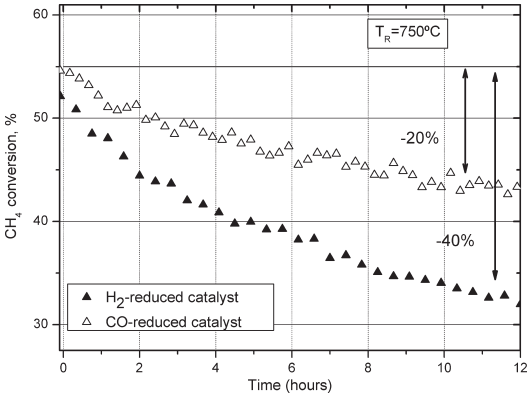

Figure 2. CH_4 conversion in the reaction of dry reforming of methane ($CH_4 + CO_2 \rightarrow 2H_2 + 2CO$) at 750 °C, using 26 wt % Ni/ZrO_2 catalyst after reduction treatments. Catalyst = 0.04 g. CH_4 and CO_2 reactants were mixed at a ratio of 1 diluted in He (10:10:80 in vol.). GHSV = 1.5×10^5 L/kg·h.

3.2. Catalytic Activity in the DRM. We have studied the catalytic performance of the catalysts after the two different reduction processes, with H_2 or CO, respectively, in the DRM reaction. Both 26 wt % Ni/ZrO_2 samples were studied for the DRM at 750 °C using an GHSV of 1.5×10^5 L/(kg· h). First of all, it is important to remark that, as verified by SEM (images not shown), under these reaction conditions, the carbon initially formed during the reduction process with CO is eliminated through the inverse Boudouard reaction ($C + CO_2 \rightarrow 2CO$) using the CO_2 from the gas mixture during the heating ramp. That means that initially at 750 °C, the catalyst surface must be free of carbon. As shown in Figure 2, the catalytic performance strongly depends on the reduction treatment. Although the initial activity is roughly the same in both systems, the catalyst previously reduced with CO presents a much higher stability, especially after 9 h in reaction conditions. After 12 h in reaction, this system loses just a 20% of the initial methane conversion, while the same catalyst reduced in hydrogen loses a 40% of activity after the same period of time. In all cases, the selectivity was stable, with values of about 0.90 for the H_2/CO ratio, close to thermodynamic values for this reaction at that temperature.

As mentioned before, several factors can influence the catalytic activity of Ni-catalysts in hydrocarbon reforming reactions. Between them, the dispersion of the nickel metallic phase is one of the most important variables affecting the catalytic performances. To characterize the size of the nickel metallic particles, we have studied the catalysts by means of XRD and XAS after being reduced with hydrogen and CO, respectively.

3.3. XRD. The crystalline phases present in the original and the reduced 26 wt % Ni/ZrO_2 catalyst were analyzed using XRD. The oxidized sample after CO reduction has also been measured to compare with the original sample. XRD patterns of every sample contain the peaks characteristic of the monoclinic structure of ZrO_2 (Figure 3), with no relevant differences between them. The main peaks corresponding to the Ni phases (oxidized and reduced) are also displayed in Figure 3. The peak at 2θ of 43.4° is characteristic of the cubic structure of NiO phase (calcined and reoxidized samples), while catalysts after CO or H_2 treatment present a peak at 2θ of 44.5°, corresponding to the cubic structure of metallic Ni phase. No other nickel phases are detected by XRD measurements.

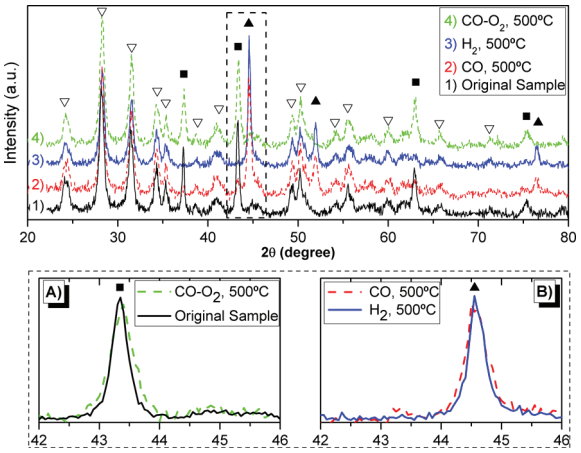

Figure 3. XRD diagrams of 26 wt % Ni/ZrO_2 system. Symbols correspond with diffraction peaks of the monoclinic ZrO_2 (▽) and cubic structures of NiO (■) and Ni^0 (▲). (A) Main Peak of cubic structure of NiO present in the calcined and reoxidized samples. (B) Main Peak of cubic structure of metallic Ni present in reduced samples.

Table 1. Crystalline Size of the NiO and Ni Phases in the 26 wt % Ni/ZrO_2 System after the Indicated Treatments, Calculated from XRD Results by Applying the Scherrer Equation

	crystalline size (nm)	
26 wt % Ni/ZrO_2	NiO	Ni
calcined	48	
H_2-reduced		46
CO-reduced		32
oxidized after CO reduction	31	

The size of the particles has been estimated from these diagrams by applying the Scherrer equation.[25] The crystalline size of the ZrO_2 phase is around 20 nm for all the samples, with no changes after the reducing and oxidizing treatments. This is not the case for the Ni particles, where significant changes have been observed in the particle sizes as a function of the reduction treatment. As it can be seen in Table 1, the original nickel oxide particles present a diameter of 48 nm. After reduction treatment, the size of the CO reduced nickel particles has decreased to 32 nm (−33%), while the reduction with hydrogen roughly maintains the initial size of the nickel particles. Moreover, this effect seems to be permanent, as after reoxidation of the CO-reduced sample, a similar size (31 nm) is obtained for the NiO particles, lower than the original ones.

3.4. SEM. To further figure out the effect of the treatment with CO decreasing the size of the metallic Ni particles, a study by SEM has been accomplished after the successive treatments with H_2, CO, and oxygen. As shown in the SEM images included in Figure 4, the original sample present two different kinds of particles. The round shape particles, with a size around 20 nm that according to the XRD data must correspond to the ZrO_2 phase, and the bigger ones, with an octahedral shape, related with the NiO phase. After H_2 treatment at 500 °C, the Ni particles appear rounded but with a similar or slightly lower size that the original NiO phase. However, after CO reduction at 500 °C, these octahedral particles evolved in smaller rounded entities,

dx.doi.org/10.1021/cs100116m |ACS Catal. 2011, 1, 82–88

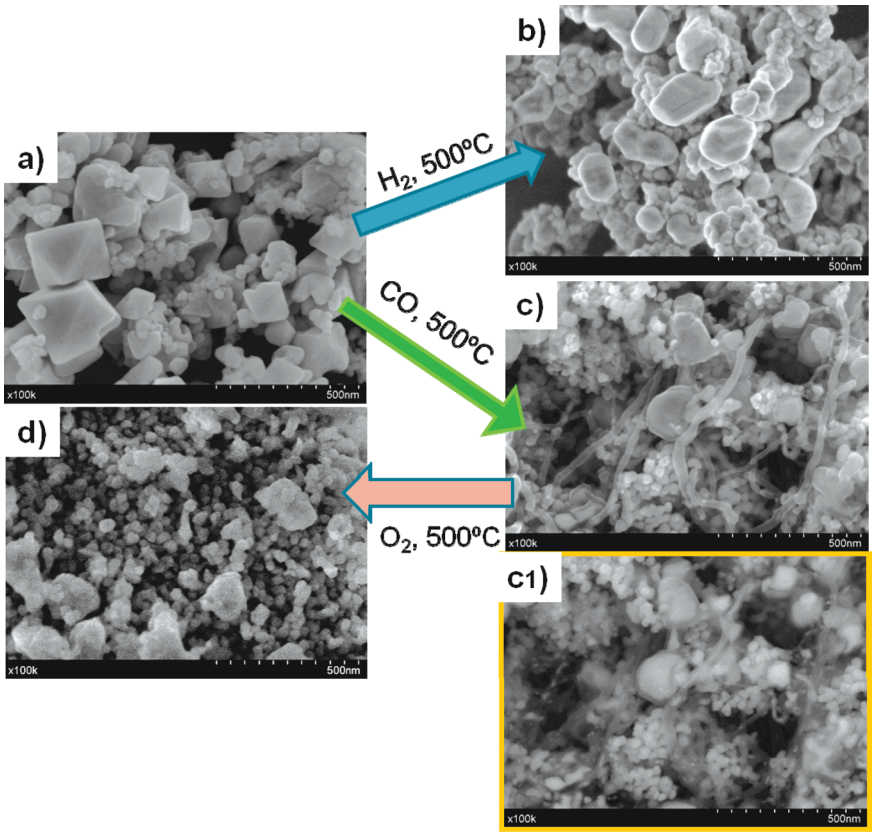

Figure 4. SEM images of the catalyst 26 wt % Ni/ZrO_2. (a) Calcined; (b) H_2 reduced sample; (c) CO reduced sample; (c1) Backscattering image of (c); (d) Oxidized sample after CO reduction.

showing that the CO treatment corrodes the nickel particles, decreasing the size of the original crystallites. Besides, the formation of carbon fibers over the catalyst is apparent, confirming the decomposition of CO via the Boudouard reaction as previously deduced from the TPR results. After the reoxidation treatment with O_2 at 500 °C, these carbon fibers disappear, without noticeable change in the shapes and sizes of the Ni/NiO particles, in agreement with the results obtained by XRD.

At this point, it must be noted that the quantitative analysis of the nickel content by ICP-MS after the reduction treatment with CO and subsequent oxidation at 500 °C, shows the same nickel content on all the samples, meaning that no losses of this metal has occurred during the treatment with CO.

3.5. XAS. The Ni particles of the 26 wt % Ni/ZrO_2 system have also been characterized by in situ X-ray Absorption during the reduction processes with CO and H_2 at 500 °C. In both cases, the spectra were collected in situ, in contact with reactive gases, after cooling down to room temperature. Ni K-edge XANES spectra obtained after the different treatment are displayed in Figure 5, where also a Ni foil spectrum has been included as a reference. The original sample presents a white line and pre-edge features similar to the massive NiO compound used as a reference (not shown). Accordingly, the XANES spectra obtained after CO and hydrogen treatment roughly correspond to a metallic nickel phase, showing that the original NiO phase has been completely reduced to Ni^0, in agreement with the TPR experiments (Figure 1) and with previous results on similar catalytic systems.[13] As described before, an important carbon formation has been detected after CO treatment (Figure 4), but no features

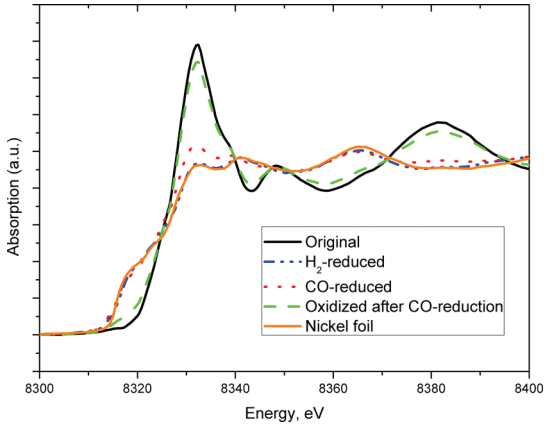

Figure 5. In situ XANES spectra of the 26 wt % Ni/ZrO_2 sample submitted to the different treatments. All the spectra have been collected after cooling down at room temperature in contact with the gas phase.

from nickel carbides or related species were detected in the XANES spectra, even though they could be easily observed in the pre-edge region of the XANES spectra.[26] The only remarkable difference between these spectra is the slightly higher white line obtained for the CO reduced sample, which must be because the spectra has been collected at room temperature, conditions allowing the surface adsorption of CO in the metallic nickel particles, slightly modifying the electronic density of the metallic nickel atoms at the particles surface. This interpretation is also confirmed with the EXAFS results shown below.

dx.doi.org/10.1021/cs100116m |*ACS Catal.* 2011, 1, 82–88

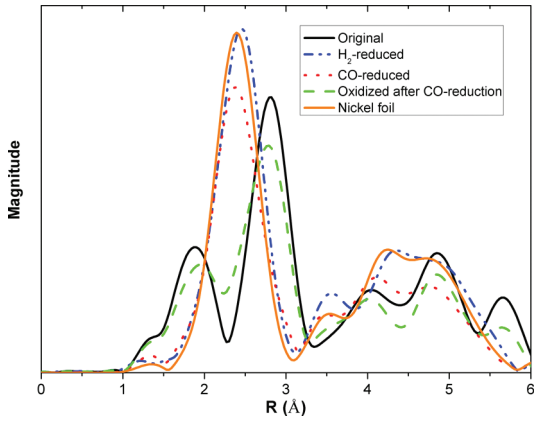

Figure 6. Fourier transform functions of the EXAFS oscillations (without phase correction) obtained for the 26 wt % Ni/ZrO_2 sample submitted to the different treatments. All the spectra have been collected after cooling down at room temperature in contact with the gas phase.

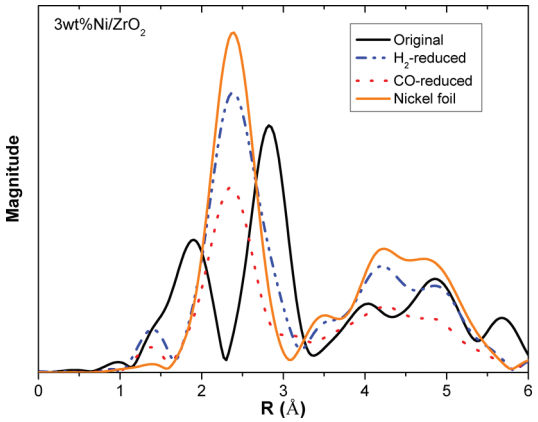

Figure 7. Fourier transform functions of the EXAFS oscillations (without phase correction) obtained for the 3 wt % Ni/ZrO_2 sample submitted to the different reduction treatments. All the spectra have been collected after cooling down at room temperature in contact with the gas phase.

Table 2. Structural Parameters for Ni Obtained by Fitting Analysis of the EXAFS Spectra of 26 wt % Ni/ZrO_2 Catalyst Submitted to the Indicated Treatments[a]

26 wt % Ni/ZrO_2	Ni−Ni (Å)	C. N.	D-W factor ($Å^2 \times 10^{-3}$)	ΔE_0 (eV)
H_2-reduced	2.48	12.0	5	5.8
CO-reduced	2.49	12.0	6	−6.8
Ni foil	2.48	12.0	5	6.7

[a] Estimated errors: Interatomic distance,<±0.02A; Coordination number (C.N.), < ±10%.

Table 3. Structural Parameters for Ni Obtained by Fitting Analysis of the EXAFS Spectra of 3 wt % Ni/ZrO_2 Catalyst Submitted to the Indicated Treatments[a]

3 wt % Ni/ZrO_2	Ni−Ni (Å)	C. N.	D-W factor ($Å^2 \times 10^{-3}$)	ΔE_0 (eV)
H_2-reduced	2.50	11.8	6	−7.0
CO-reduced	2.49	10.2	9	−2.3
Ni foil	2.48	12.0	5	6.7

[a] Estimated errors: Interatomic distance,<±0.02A; Coordination number (C.N.), < ±10%.

The Fourier transformed (FT) functions obtained from the EXAFS oscillations of the XAS spectra are presented in Figure 6 (without phase shift corrections). Once again, the FT functions of the oxidized samples are typical for NiO systems, with two main peaks below 3.5 Å. Also, those obtained after the reduction processes indicate the presence of metallic nickel, confirming the nickel has been completely reduced after the CO and hydrogen treatments. No peaks from oxidized nickel phases are detected. Although some differences in the intensity of the main peak at 2.4 Å could be observed between the samples reduced with CO or hydrogen, the fitting analysis shows similar structural parameters for both systems. After these fitting results, included in Table 2, in both cases the main peak centered at around 2.4 Å, corresponding to the first Ni−Ni coordination shell of metallic nickel, yields 12 neighbors atoms at 2.49 Å, so H_2 or CO reduction give particles with the same coordination number (C.N. = 12). The only remarkable differences come from the Debye−Waller factors, slightly higher for the Ni particles obtained after reduction with CO, which can be related with a slightly more disordered structure. As the coordination number of the first shell in metals can be used for determining the average particle size,[27] this value of C.N. = 12 indicates that the Ni particles are in both cases larger than 10 nm, in agreement with the particle size previously deduced from XRD. So, with such big particles, it is not possible to determine differences in size by XAS.

For this reason, we have prepared and characterized by in situ XAS a similar Ni/ZrO_2 catalyst but with a lower Ni content (wt. 3%). It is worthy to note that in this catalyst no peaks from nickel phases could be observed by XRD for the oxidized or the CO reduced sample. However, the hydrogen reduced one shows a small peak at 2θ of 44.5°, but so tiny and overlapped with peaks from the zirconia phase that it does not allow the quantification with the Scherrer equation. Hence, these results show qualitatively a similar behavior of the nickel phase than that previously observed in the high loaded sample. Figure 7 shows the FT functions obtained from the EXAFS region of the XAS spectra of this 3%Ni/ZrO_2 system before and after reduction with CO or hydrogen. The visual inspection of these FT functions clearly shows as the H_2-reduced sample presents a Ni−Ni coordination shell (centered at 2.36 Å without phase correction) much more intense that the CO-reduced one. According to the parameters obtained by fitting analysis (Table 3), these peaks correspond to a coordination number of about 12 in the first case, but just 10 in the catalyst reduced with CO, indicating that the average crystallite size of nickel is much larger when reduced with hydrogen. In accordance with other authors,[28−30] a C.N. of 12 is associated with particles larger than 10 nm in size, while a C.N. of 10 corresponds to particle sizes around 4 nm. Thus, these data are also in agreement with the behavior observed previously by XRD for the catalyst with a higher loading of Ni, confirming that Ni particles after CO reduction present a lower size than particles reduced with hydrogen. Therefore, the treatment with CO strongly disperses the metallic particles of nickel from dispersion values lower than 10% (C.N. = 12) to values around 20% (C.N. = 10), showing that the dispersion effect appears irrespective of the nickel content in the catalytic system.

dx.doi.org/10.1021/cs100116m |*ACS Catal.* 2011, 1, 82–88

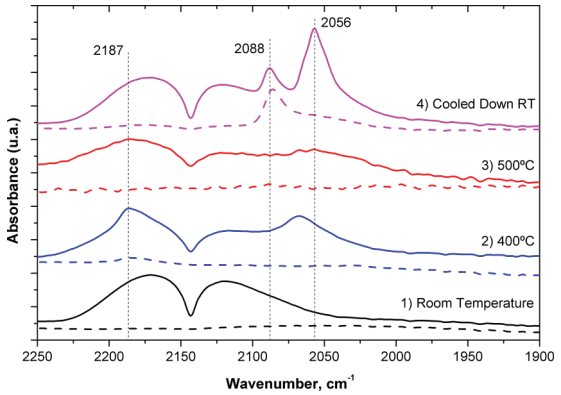

Figure 8. FTIR spectra of the 3 wt % Ni/ZrO_2 sample during reduction treatment with CO. All the spectra have been collected at the indicated temperature, in contact with the gas phase. Solid lines: Spectra under CO atmosphere (Gas mixture: 5% CO/Ar). Dash: Spectra after CO evacuation.

At this time, it is important to remark that in both cases, these 3%Ni/ZrO_2 catalysts are almost inactive for the dry reforming of methane, reaching less than 10% conversion of the hydrocarbon. This finding agrees with the well-known fact that well dispersed nickel particles are prone to coke formation, yielding less stable catalysts for hydrocarbon reforming reactions[31,32]. As it is also known that very big nickel particles are also easily poisoned with coke, it means that, depending on the size range of the particles, an increase in the dispersion of big particles could increase the resistance to poisoning, as it seems to be the case for the 26 wt % Ni/ZrO_2 system.

3.6. DRIFTS. The mechanism of this dispersion process can be understood from the FTIR results obtained for the 3 wt % Ni/ZrO_2 sample, included in Figure 8. These spectra have been obtained by in situ DRIFTS during the reduction treatment with CO. As shown, when the sample is in contact at room temperature with 50 Torr of CO, only gas-phase CO bands are detected, which disappear after CO evacuation. By treatment with CO, at the temperature of 400 °C a band centered at 2067 cm^{-1} arises which according to the literature must be related with the formation of nickel carbonyl species.[33−35] This IR band is almost completely reversible, as it vanishes after evacuation at 400 °C. Also, another band at 2187 cm^{-1} can be observed, which in accordance with Resini et al.[36] can be assigned to CO adsorbed in Zr^{4+} Lewis acidic sites or to carbonyls of Ni^{2+}-CO type. The 3 wt % Ni/ZrO_2 sample previously reduced and the ZrO_2 used as support have been measured in the same conditions (results not shown). In these measurements the band at 2187 cm^{-1} does not appear at 400 °C, therefore indicating that this band is probably associated to the adsorption of CO over oxidized Ni^{2+} species. As shown, this band is not completely reversible after evacuating at 400 °C, which agrees with the known high stability of this Ni^{2+}-CO species. The fact that this band is not detected in the original oxidized sample can be related with the presence of surface contamination (physisorbed water and carbonates species) covering the nickel particles.

The CO adsorption at 500 °C must reduce the nickel, and produces just two weak, reversible bands at around 2056 and 2088 cm^{-1}. After cooling down to room temperature in the presence of CO, two intense bands could be easily detected: the first one at 2088 cm^{-1}, which remains after evacuating the CO, and the second at 2056 cm^{-1} almost completely reversible by evacuation. According to Mihaylov et al.,[37] the irreversible band at 2088 cm^{-1} is related with CO adsorbed on dispersed Ni^0, while the reversible band at 2056 cm^{-1} would be associated to physisorbed nickel carbonyl species. As the ICP analysis have shown no losses of nickel from the catalyst during the CO treatment, the formation of these $Ni(CO)_4$ could accounts for the dispersion process of nickel, via formation of the tetracarbonyl complex and gas phase transfer to the surrounding regions on the zirconia support. As these nickel carbonyl species do not fly away from the catalyst through the gas phase, they must decompose over the support, leaving the nickel species on the zirconia surface. This fact shows an important interaction between the nickel entities and the zirconia support. As indicated in Scheme 1, the process must proceed by the initial surface reduction of the nickel oxide particles, the subsequent formation of the tetracarbonyl complexes with these metallic atoms from the surface, which through the gas phase, are readsorbed on the support nearby the original particle. The final result is the corrosion of the original particle, in agreement with the SEM images, and the decrease of the particle size. With hydrogen, the reduction process is directly accomplished over the nickel oxide particle, resulting in a metallic size similar to the original oxidized one.

Scheme 1. Schematic Evolution of the Shape of the Nickel Particles Submitted to a Reducing Treatment with CO[a]

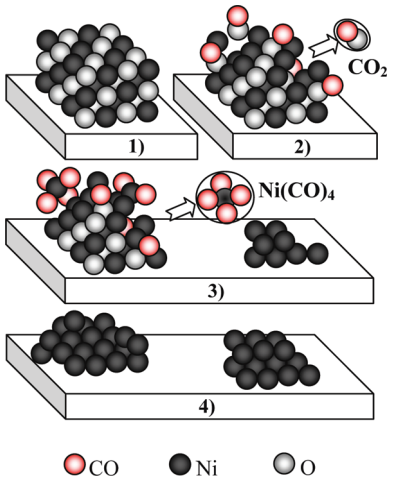

[a] (1) NiO particle; (2) CO molecules react with Oxygen atoms of NiO producing CO_2. (3) When the particle is partially reduced, some CO molecules form tetracarbonyls with nickel atoms, depositing the metal atoms around onto the support. (4) Finally, metallic particles of Ni show a smaller size than the original particle of NiO.

4. CONCLUSIONS

Our results clearly indicate that by comparing the reduction processes with H_2 or CO at 500 °C on Ni/ZrO_2 catalysts, the first one does not noticeably modify the size of the original nickel oxide phase, while a similar reduction treatment with CO clearly decreases the size of the particles, modifying the dispersion of the metallic nickel phase in the catalyst, which explains the better catalytic stability of the CO reduced catalyst in the methane dry reforming reaction. This different behavior during the reduction process can be understood considering the formation of $Ni(CO)_4$ complexes during the reduction with CO, which corrodes the nickel particles, decreasing their size and depositing the metal atoms around onto the support. This gas phase process

dx.doi.org/10.1021/cs100116m |ACS Catal. 2011, 1, 82–88

occurs without measurable losses of nickel from the catalyst. This seems to be in contradiction with the findings of others authors[16−19] that reported the sintering of the nickel particles and/or the loss of metal from the catalyst during other related reactions as methanation of CO or methanol carbonylation. These studies refer to catalyst of nickel supported on silica, alumina, or carbon. From our results, these differences could be explained according to differences in the interaction of nickel with the support surfaces. In our Ni/ZrO_2 catalysts, as the nickel content do not decrease during the CO treatment, it must indicate that the nickel carbonyl species do no fly away but collide with the zirconia surface, where the carbonyl species decompose, leaving the nickel atoms on the near surface and so, increasing the dispersion of the metal particles within the optimal range to improve the catalytic performance.

AUTHOR INFORMATION

Corresponding Author
*E-mail: caballero@us.es.

ACKNOWLEDGMENT

We thank the Ministry of Education and Science of Spain and the Junta de Andalucia for financial support (Projects ENE2007-67926-C02-01 and P07-FQM-02520), the ESRF facility and the BM25 Spline beamline staff for their experimental support.

REFERENCES

(1) Gadalla, A. M.; Bower, B. *Chem. Eng. Sci.* **1988**, *43*, 3049–3062.
(2) Ross, J. R. H.; van Keulen, A. N. J.; Hegarty, M. E. S.; Seshan, K. *Catal. Today* **1996**, *30*, 193–199.
(3) Rostrup-Nielsen, J. R.; Bak Hansen, J. H. *J. Catal.* **1993**, *144*, 38–49.
(4) Bradford, M. C. J.; Vannice, M. A. *Appl. Catal., A* **1996**, *142*, 73–96.
(5) Zhang, Z.; Verykios, X. E. *Appl. Catal., A* **1996**, *138*, 109–133.
(6) Armor, J. N. *Appl. Catal., A* **1999**, *176*, 159–176.
(7) Lee, D.; Hacarlioglu, P.; Oyama, S. T. *Top. Catal.* **2004**, *29*, 45–57.
(8) Zhang, W. D.; Liu, B. S.; Zhan, Y. P.; Tian, Y. L. *Ind. Eng. Chem. Res.* **2009**, *48*, 7498–7504.
(9) Gonzalez-Delacruz, V. M.; Ternero, F.; Pereñiguez, R.; Caballero, A.; Holgado, J. P. *Appl. Catal., A* **2010**, *384*, 1–9.
(10) Bradford, M. C. J.; Vannice, M. A. *Catal. Rev. Sci. Eng.* **1999**, *41*, 1–42.
(11) Wei, J.; Iglesia, E. *J. Catal.* **2004**, *224*, 370–383.
(12) Tang, S.; Ji, L.; Lin, J.; Zeng, H. C.; Tan, K. L.; Li, K. *J. Catal.* **2000**, *194*, 424–430.
(13) Gonzalez-Delacruz, V. M.; Holgado, J. P.; Pereñiguez, R.; Caballero, A. *J. Catal.* **2008**, *257*, 307–314.
(14) Barroso-Quiroga, M. M.; Castro-Luna, A. E. *Int. J. Hydrogen Energy* **2010**, *35*, 6052–6056.
(15) Caballero, A.; Holgado, J. P.; Gonzalez-delaCruz, V. M.; Habas, S. E.; Herranz, T.; Salmeron, M. *Chem. Commun.* **2010**, *46*, 1097–1099.
(16) Shen, W. M.; Dumesic, J. A.; Hill, C. G., Jr. *J. Catal.* **1981**, *68*, 152–165.
(17) Agnelly, M.; Kolb, M.; Mirodatos, C. *J. Catal.* **1994**, *148*, 9–21.
(18) Martra, G.; Swaan, H. M.; Mirodatos, C.; Kermarec, M.; Louis, C. *Stud. Surf. Sci. Catal.* **1997**, *111*, 617–624.
(19) Yao, S.; Yang, C.; Tan, Y.; Han, Y. *Catal. Commun.* **2008**, *9*, 2107–2111.
(20) Caballero, A.; Morales, J. J.; Cordon, A. M.; Holgado, J. P.; Espinos, J. P.; Gonzalez-Elipe, A. R. *J. Catal.* **2005**, *235*, 295–301.
(21) Malet, P.; Caballero, A. *J. Chem. Soc., Faraday Trans.* **1988**, *84*, 2369–2375.
(22) Pereñiguez, R.; González-DelaCruz, V. M.; Caballero, A.; Holgado, J. P. *Appl. Catal., B* **2010**, *93*, 346–353.
(23) Newville, M. *J. Synchrotron Radiat.* **2001**, *8*, 322–324.
(24) Ravel, B. *J. Alloys Compd.* **2005**, *401*, 118–126.
(25) Patterson, A. L. *Phys. Rev.* **1939**, *56*, 978–982.
(26) Takenaka, S.; Shigeta, Y.; Tanabe, E.; Otsuka, K. *J. Phys. Chem. B* **2004**, *108*, 7656–7664.
(27) Jentys, A. *Phys. Chem. Chem. Phys.* **1999**, *1*, 4059–4063.
(28) Frenkel, A. I.; Hills, C. W.; Nuzzo, R. G. *J. Phys. Chem. B* **2001**, *105*, 12689–12703.
(29) de Graaf, J.; van Dillen, A. J.; de Jong, K. P.; Koningsberger, D. C. *J. Catal.* **2001**, *203*, 307–321.
(30) Miller, J. T.; Kropf, A. J.; Zha, Y.; Regalbuto, J. R.; Delannoy, L.; Louis, C.; Bus, E.; van Bokhoven, J. A. *J. Catal.* **2006**, *240*, 222–234.
(31) Takenaka, S.; Kobayashi, S.; Ogihara, H.; Otsuka, K. *J. Catal.* **2003**, *217*, 79–87.
(32) Li, Y.; Zhang, B.; Xie, X.; Liu, J.; Xu, Y.; Shen, W. *J. Catal.* **2006**, *238*, 412–424.
(33) Yates, J. T.; Garland, C. W. *J. Phys. Chem.* **1961**, *65*, 617–624.
(34) Hadjiivanov, K.; Mihaylov, M.; Klissurski, D.; Stefanov, P.; Abadjieva, N.; Vassileva, E.; Mintchev, L. *J. Catal.* **1999**, *185*, 314–323.
(35) Poncelet, G.; Centeno, M. A.; Molina, R. *Appl. Catal., A* **2005**, *288*, 232–242.
(36) Resini, C.; Venkov, T.; Hadjiivanov, K.; Presto, S.; Riani, P.; Marazza, R.; Ramis, G.; Busca, G. *Appl. Catal., A* **2009**, *353*, 137–143.
(37) Mihaylov, M.; Hadjiivanov, K.; Knözinger, H. *Catal. Lett.* **2001**, *76*, 59–63.